Chapter 4

Magnetic Dichroism in Photoemission from Atoms

The growing interest in using magnetic materials for practical applications stimulates the ongoing research in the magnetic and electronic structure of solids. A particularly powerful method in this respect is spin-polarized photoemission. Here, the spin of the outgoing photoelectron is monitored in addition to the parameters ($k_{\|}$, E) measured in conventional PE. A disadvantage of this method is the low detection efficiency [29].

Magnetic dichroism in PE is an alternative way to obtain information on the magnetic state of a sample. Magnetic dichroism in PE originates from the fact that dipole-transition matrix elements depend on the magnetic quantum number of the electron in the initial state and parameters of the incident radiation (polarization, angle). Different choices of the incident radiation field and initial state will lead to different transition probabilities into a particular final state. Therefore, in appropriately chosen experimental geometries, a change in sample magnetization $\vec{M}$ as well as in $\vec{q}$ (CP light) or in $\vec{E}$ (LP light) will lead to a variation in PE line intensity that is commonly referred to as magnetic dichroism in PE. We shall illustrate this for PE from an atom in two different cases: in the first case one can describe the electron in a one-electron picture, in the second case one has to use atomic multiplet theory (many-body description).

The theory of PE dichroism of rare-earth elements has been addressed in part in a number of papers [30–34]. Here, we shall concentrate on the case of rare-earth elements investigated in this work. After a brief presentation of an appropriate description of lanthanide 4f levels, we shall briefly present the effects of ground-state splitting and dipole selection rules on the dipole transition matrix elements, as well as their dependence on light helicity and sample magnetization.

4.1 Experimental geometries for magnetic dichroism

In magnetic dichroism PE experiments one needs four quantities to uniquely define the system:

$$\left\{\vec{q}, \vec{M}, \vec{e}_{em}, \vec{e}_{x,y,z}\right\}.$$

Vector $\vec{q}$ describes the incoming radiation. It denotes the orientation of photon momentum (circularly polarized light) or the polarization vector (linearly polarized light). $\vec{M}$ is the magnetization of the sample, $\vec{e}_{em}$ the emission direction of the photoelectrons. For crystalline samples, we also need the crystal lattice $\vec{e}_{x,y,z}$ to uniquely define the system.

The first two vectors are 'inherited' from x-ray absorption spectroscopy (XAS), where XMCD signals scale with the inner product $\vec{q} \cdot \vec{M}$, and these two values are sufficient to define the XMCD system. In PE, the vector $\vec{e}_{em}$ enters as a result of the angle-resolved detection of the photoelectron; it is also needed to define the crystal orientation in order to account for photoelectron diffraction effects. Altogether, angular resolution in PE reduces the symmetry of the system compared to XAS, and hereby allows one to observe magnetic dichroism (MD) in additional experimental geometries. Yet, as it often happens, it also makes the analysis more difficult as compared to MD in XAS, where the MD signal is simply proportional to the inner product $\vec{q} \cdot \vec{M}$.

According to Feder and Henk [35], a necessary condition for the presence of MD effects in some particular geometries is: ***no space-symmetry operation should exist that reverses the magnetization but leaves the system unchanged otherwise***. This statement is valid for XAS as well PE experiments.

Magnetic dichroism in PE can be observed with circularly polarized light. However, it was demonstrated that MDPE can also be observed with linearly p-polarized light (described by $\vec{E}$), when the vectors span a 'chiral' geometry [32, 36, 37], i.e. when

$$\left|\vec{E}(\vec{M} \times \vec{k})\right| > 0. \tag{4.1}$$

We have used this chiral geometry for magnetic linear dichroism (MLD) experiments in the present work.

In the following, we shall briefly review the one-electron theory to provide a transparent picture of the mechanism underling the MD effect in the atomic case. Here we follow the approach of Menchero [38] that was successfully used to describe MD in PE from deeper core levels (2p, 3p, 4d). Although the many-body approach is commonly accepted to be better in describing PE from 4f shells (see sects. 4.3), the one-electron picture is more transparent.

4.2 Single particle model

Let us regard the PE process from an oriented atom. The situation of a magnetic solid is included by assuming an exchange splitting of the different sublevels. The geometry of the PE process is illustrated in Fig. 4.1.

The idea is to express the dipole operator, the initial and the final states in terms of the well-known spherical harmonics; this will allow a simple treatment

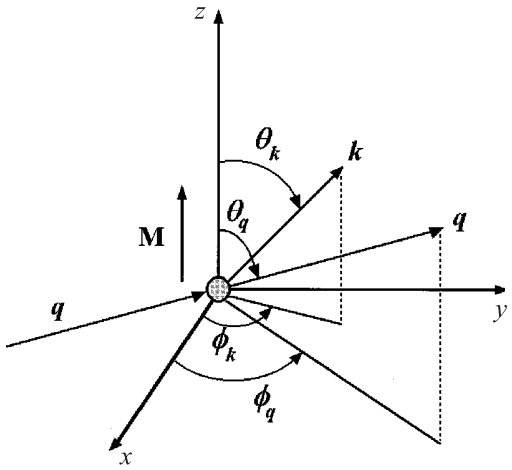

Figure 4.1: Measurement geometry for PE. The atom is magnetized along the z direction. Index k denotes the photoelectron parameters (with wave vector $\vec{k}$); index q indicates photon parameters; from Ref. [39].

of a general photon-incidence direction and polarization to describe the PE process. Since all parameters have an obvious physical meaning (emission angle of electrons, photon polarization, etc.), this formalism has the beauty of being transparent and straightforward, and it allows to perform calculations by hand (see Appendix A).

According to Fermi's Golden rule, the intensity of PE lines is given by

$$I^{\epsilon}_{k\sigma} = \left| \left\langle \Psi^f_{k\sigma} \right| T_\epsilon \left| \Psi^i \right\rangle \right|^2 \delta(E_b + E_k - \hbar\omega), \tag{4.2}$$

where the δ-function ensures energy conservation; ϵ describes the photon polarization; k and σ denotes wave vector of electron and its spin, respectively. The general expression for the dipole operator, depending on the photon incidence direction and light polarization, is derived in Appendix A. Here, we just reproduce the final expression:

$$T_\epsilon = \vec{r} \cdot \vec{\epsilon} = r\sqrt{\frac{4\pi}{3}} \left(-Y_1^1 \epsilon_+ + Y_1^{-1} \epsilon_- + Y_1^0 \epsilon_z \right), \tag{4.3}$$

with the light polarization described by the components (Appendix A)

$$\begin{aligned} \epsilon_+ &= \frac{e^{-i\phi_q}}{\sqrt{2}} [\cos\alpha \ \cos\theta_q - i \sin\alpha e^{i\delta}] \\ \epsilon_- &= \frac{e^{i\phi_q}}{\sqrt{2}} [\cos\alpha \ \cos\theta_q + i \sin\alpha e^{i\delta}] \\ \epsilon_z &= -\cos\alpha \ \sin\theta_q. \end{aligned} \tag{4.4}$$

The photon propagation direction is defined by $(\theta_q, \ \phi_q)$ and the unit vector of light polarization is given by the angles α and δ.

As an illustration, RCP light propagating in z direction ($\theta_q = 0^0$, see Fig. 4.1) with $\alpha = 45^0$ and $\delta = 90^0$ ($|\epsilon_+| = 1$) corresponds to $T_\epsilon \propto Y_1^1$, i.e. the photon angular momentum and wave vector $\vec{q}$ are parallel. LP light propagating along x direction ($\theta_q = 90^0,\ \phi_q = 0^0$) with $\alpha = 90^0$, $\delta = 0^0$ ($\hat{\epsilon} = \hat{e}_y$) gives $\epsilon_+ = -i/\sqrt{2}$ and $\epsilon_- = i/\sqrt{2}$, corresponding $T_\epsilon \propto i\left(Y_1^1 + Y_1^{-1}\right) \propto y$.

The PE final state with emission direction $\vec{k}$ can be represented by a superposition of spherical waves and written in the basis of spherical functions [40]:

$$\Psi^f_{k\sigma}(r,\theta,\phi) = 4\pi \sum_{lm} i^l e^{-i\delta_l} Y^*_{lm}(\theta_k,\phi_k) Y_{lm}(\theta,\phi) f_{kl}(r)\sigma, \tag{4.5}$$

with the phase shift δ_l for outgoing waves and an energy-dependent radial wave function $f_{kl}(r)$.

The electron wave function of the initial state can be decomposed in a radial and an angular part, including spin dependence:

$$\left|\Psi^i\right\rangle = \left|f_{nl}(r),\ \Phi_\sigma(\theta,\phi)\right\rangle. \tag{4.6}$$

To define $\Phi_\sigma(\theta,\phi)$, we follow the approach introduced by G. van der Laan [41]. The Hamiltonian includes spin-orbit interaction and exchange interaction by means of a spin field,

$$H = \lambda \vec{l}\cdot\vec{s} + \xi s_z. \tag{4.7}$$

The first term accounts for the spin-orbit coupling with strength λ, the second is due to exchange. The basis set is chosen as $|j,m_j\rangle$, consisting of eigenfunctions of the $\vec{l}\cdot\vec{s}$ operator. The spin operator s_z couples the m_j states allowing a mixing between the $j = l + 1/2$ and $j = l - 1/2$ states. Thus, only m_j (not j) is a good quantum number, which means that the system is invariant under rotation about $\vec{M}$.

One should now define the angular and the spin part of the wave function $|j,m_j\rangle$ of a spin $\frac{1}{2}$ particle that is in the state of orbital moment l. Mathematically, this is achieved by coupling the angular momenta, one for the spin and another one for the orbital momentum. It can be viewed as a transformation between the two basic sets of wave functions $|j,m_j\rangle$ and $|m_l,m_s\rangle$, performed by a transformation matrix that can be constructed from Clebsh-Gordan coefficients (note that the full notation is $|l,s,m_l,m_s\rangle$ and $|l,s,j,m_j\rangle$). To be specific, let us consider the case $l = 1$. In this case one obtains for $|j,m_j\rangle$ the following linear combinations

$$\begin{aligned}
|3/2,\ \ 3/2\rangle &= \left|Y_1^1\uparrow\right\rangle \\
|3/2,\ \ 1/2\rangle &= \sqrt{2/3}\left|Y_1^0\uparrow\right\rangle + \sqrt{1/3}\left|Y_1^1\downarrow\right\rangle \\
|3/2,-1/2\rangle &= \sqrt{1/3}\left|Y_1^{-1}\uparrow\right\rangle + \sqrt{2/3}\left|Y_1^0\downarrow\right\rangle \\
|3/2,-3/2\rangle &= \left|Y_1^{-1}\uparrow\right\rangle \\
|1/2,\ \ 1/2\rangle &= \sqrt{1/3}\left|Y_1^0\uparrow\right\rangle - \sqrt{2/3}\left|Y_1^1\downarrow\right\rangle \\
|1/2,-1/2\rangle &= \sqrt{2/3}\left|Y_1^{-1}\uparrow\right\rangle - \sqrt{1/3}\left|Y_1^0\downarrow\right\rangle.
\end{aligned} \tag{4.8}$$

To express the matrix elements of Hamiltonian (4.7) one also needs the expansion of the $|j, m_j\rangle$ states in $|m_l, m_s\rangle$ basis functions to find out how the $\vec{l} \cdot \vec{s}$ and s_z operators act on the $|j, m_j\rangle$ states. With this, it is straightforward to show that the Hamiltonian takes the form:

$$H = \frac{1}{6} \begin{pmatrix} 3\lambda + 3\xi & 0 & 0 & 0 & 0 & 0 \\ 0 & 3\lambda + \xi & 0 & 0 & \sqrt{8}\xi & 0 \\ 0 & 0 & 3\lambda - \xi & 0 & 0 & \sqrt{8}\xi \\ 0 & 0 & 0 & 3\lambda - 3\xi & 0 & 0 \\ 0 & \sqrt{8}\xi & 0 & 0 & -6\lambda - \xi & 0 \\ 0 & 0 & \sqrt{8}\xi & 0 & 0 & -6\lambda + \xi \end{pmatrix}. \quad (4.9)$$

The appearance of off-diagonal terms directly shows the mixing of the $j = 3/2$ and $j = 1/2$ states with equal m_j numbers. As it has been mentioned above, m_j stays to be a good quantum number due to the preserved rotational symmetry around the magnetization axis.

The resulting scheme of levels is illustrated on Fig. 4.2 in the limit of $\lambda \gg \xi$. In this limit, $p_{3/2}$ and $p_{1/2}$ energy levels are given by:

$$E_i = \begin{cases} \frac{\lambda}{2} + \frac{\xi}{3} m_j, & j = \frac{3}{2} \\ -\lambda - \frac{\xi}{3} m_j & j = \frac{1}{2} \end{cases}. \quad (4.10)$$

The Hamiltonian matrix in Eq. 4.9 has to be diagonalized to obtain the eigenstates $\Phi_\sigma(\theta, \phi)$ for arbitrary λ, ξ. The eigenfunctions will be presented as linear combinations of $|j, m_j\rangle$ states with the same m_j. This mixing becomes negligible for the case of $\lambda \gg \xi$.

To calculate the transition matrix element for the general case, it is sufficient to write it as a linear combination of the matrix elements calculated for the $|j, m_j\rangle$ basis states. The matrix elements for the three basic electric-dipole operators in Eq. 4.3 can be calculated analytically and were tabulated by Menchero [38]; they are reproduced in Appendix A (Table A.1, A.2, A.3).

Let us now turn to a typical core-level MDPE experiment in the limit of $\lambda \gg \xi$. Dichroism can be measured by reversal of the sample magnetization in two subsequent experiments, and the PE line intensity difference $I_{up} - I_{down}$ represents the magnetic dichroism effect; it is illustrated in Fig. 4.2. In the limit of $\lambda \gg \xi$, the core levels are given by $|j, m_j\rangle$ spin-orbit eigenstates; adjacent m_j levels are separated in energy by $\xi/3$. In this limit, a reversal of the magnetization will reverse the positions of $|j, m_j\rangle$ and $|j, -m_j\rangle$ levels, without affecting their intensities in PE.

For the case of CP excitation ($\vec{q} \parallel \vec{M}$), the MD can be written as

$$\begin{aligned} 2p_{3/2}: \; I_{|3/2,3/2\rangle} - I_{|3/2,-3/2\rangle} &= 3\Delta_{MCD}(\theta_k, \phi_k) \\ I_{|3/2,1/2\rangle} - I_{|3/2,-1/2\rangle} &= \Delta_{MCD}(\theta_k, \phi_k) \\ 2p_{1/2}: \; I_{|1/2,1/2\rangle} - I_{|1/2,-1/2\rangle} &= 2\Delta_{MCD}(\theta_k, \phi_k). \end{aligned} \quad (4.11)$$

The angular dependence of the MD effect is contained in the quantity

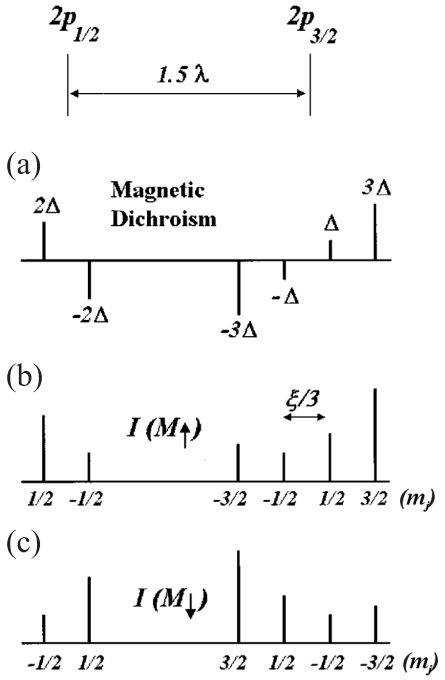

Figure 4.2: (a) Illustration of magnetic dichroism for p-level photoemission in the limit $\lambda \gg \xi$. (b) and (c) Relative intensities and energy positions of m_j-components in the PE spectra upon magnetization reversal; from Ref. [38].

$$\Delta_{MCD}(\theta_k, \phi_k) = \frac{1}{3}\left(3R_2^2 \sin^2\theta_k - R_0^2 - R_2^2 - R_0 R_2 \left(3\cos^2\theta_k - 1\right)\cos(\delta_0 - \delta_2)\right). \tag{4.12}$$

When using linearly polarised light in a chiral experimental geometry, MD has the same appearance

$$\begin{aligned} 2p_{3/2}: \; I_{|3/2,3/2\rangle} - I_{|3/2,-3/2\rangle} &= 3\Delta_{MLD}(\theta_k, \phi_k) \\ I_{|3/2,1/2\rangle} - I_{|3/2,-1/2\rangle} &= \Delta_{MLD}(\theta_k, \phi_k) \\ 2p_{1/2}: \; I_{|1/2,1/2\rangle} - I_{|1/2,-1/2\rangle} &= 2\Delta_{MLD}(\theta_k, \phi_k), \end{aligned} \tag{4.13}$$

yet with

$$\Delta_{MLD}(\theta_k, \phi_k) = R_0 R_2 \sin^2\theta_k \sin 2\phi_k \sin(\delta_0 - \delta_2). \tag{4.14}$$

Comparing the spectral shapes in (4.11) and (4.13), we arrive at the important conclusion: ***the shape of MLD is equal to the shape of MCD***. However, this does not hold for the size and angular dependence. Although we have derived this result in the framework of a one-electron model (in the limit $\lambda \gg \xi$) it is valid more generally for any λ and ξ. Moreover, and this is especially important for us, it also holds for MD from localized 4f shells, where the many-body approach is needed.

The possibility to observe MD with unpolarized light also can be expected, if one views it as an incoherent superposition of s- and p-components (due to the p-component, since the s-component does not contribute to MD).

It is instructive to point out that MD can be qualitatively viewed as the result of spin-polarized emission induced by the excitation field (e.g. CP light). At certain emission angles and chosen level, one spin component can have a higher excitation probability, e.g. the spin-up orientation (minority character). Upon reversal of magnetization, the spin-up electrons will still be exited with higher probability, but now the same level has majority character. The change from minority to majority character is accompanied by an increase of the binding energy. LP light can also lead to an induced spin polarization, and consequently to an MD effect.

Another useful result of the single-particle model is the following: ***reversal of magnetization and reversal of helicity are equivalent only in certain geometries***, e.g. when $\vec{M}$, $\vec{q}$ and $\vec{k}$ are coplanar.

Let us consider a sample with the surface normal oriented in x-direction, which is magnetized in z-direction. Let the photon be incident in the xz plane ($\theta_q = 45^0,\ \phi_q = 180^0$), and concentrate on normal emission ($\theta_k = 90^0,\ \phi_k = 0^0$). The asymmetry upon *magnetization reversal* can be defined by

$$A = \frac{\sum_n \left| I_n^{M_{up}} - I_n^{M_{down}} \right|}{\sum_n (I_n^{M_{up}} + I_n^{M_{down}})}, \tag{4.15}$$

where the summation is over n multiplet lines. Simply speaking, the asymmetry A is given by the area under the difference spectrum divided by the area under the sum of the spectra.

For MD experiments with CP light, where the sample magnetization is fixed but the *light helicity* is switched, the asymmetry is given by:

$$\widetilde{A} = \frac{\sum_n \left| I_n^{RCP} - I_n^{LCP} \right|}{\sum_n (I_n^{RCP} + I_n^{LCP})}. \tag{4.16}$$

Both asymmetries, A and $\widetilde{A}$, are equal for the highly symmetric geometries chosen above. But the equivalence of the two definitions does not hold in general. When reducing the symmetry of the experiment, e.g. by rotating the magnetization $\vec{M}$ around the surface normal (so that it is still in the yz-plane), A and $\widetilde{A}$ are no longer identical. This is illustrated in Fig. 4.3, where the magnetic dichroic asymmetries are shown as a function of the rotation angle β for the cases of RCP, LCP, s-, and p-polarized excitation (with parameters $R_2/R_0 = 3$ and a phase difference $\delta_2 - \delta_0 = 1$). The case of $\beta = 0$ corresponds to $\vec{M} \parallel z$-axis in Fig. 4.1.

In case of LP light, the dichroic asymmetry A_p (p-polarized excitation) is non-vanishing, reaching a maximum value for $\beta = 90^0$ (i.e. $\vec{M} \parallel y$-axis). For p-polarized excitation, MD is originating entirely from cross-channel interference (Eq. 4.14). This is indicated by the proportionality of the overall dichroic signal intensity to the sine function of the phase-shift difference for two excited waves.

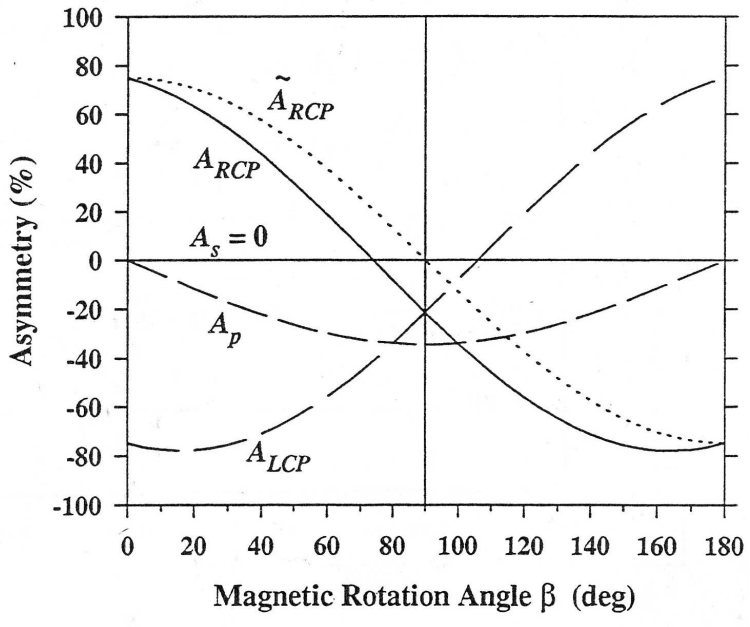

Figure 4.3: Dichroic asymmetries for CP and LP incident radiation plotted as angular dependence on the magnetic rotation angle β (see text). LP light: Asymmetries are shown for s- and p-type polarization (A_s, A_p). CP light: Asymmetries corresponding to magnetization reversal (A_{RCP}, A_{LCP}) and flip of photon helicity ($\widetilde{A}$); from Ref. [38].

As will be seen in section 4.4, this also holds for MD in PE from the 4f shells. For s-polarized light, the dichroic asymmetry A_s is always zero.

The consequence of cross-channel interference is that $A_{RCP} \neq A_{LCP}$, as can be seen directly from the angular dependences shown in Fig. 4.3. Indeed, the dichroism observed with unpolarized light would disappear, if A_{RCP} and A_{LCP} are equivalent (viewing unpolarized light as an incoherent superposition of RCP and LCP components). At the same time unpolarized excitation, as was mentioned above, can be regarded as an incoherent superposition of s- and p-components. Since s-polarized excitation does not contribute to MD, a vanishing MD would imply that A_p should also be zero. However, in general this is not the case, i.e. MD for p-light does not vanish due to cross-channel interference. From all of this it is evident that A_{RCP} and A_{LCP} cannot be equal.

For the general case one can write

$$A_{RCP}(90^0 + \eta) = A_{LCP}(90^0 - \eta) \tag{4.17}$$

where η denotes the angle of rotation from $\beta = 90^0$.

It can be seen in Fig. 4.3 that **MD asymmetry from an experiment where the *photon helicity is reversed deviates in general from the MD asymmetry obtained from an experiment where the magnetization is***

reversed. Only for $\beta = 0^0$ and 180^0 the dichroism is equivalent. For $\beta = 90^0$, due to symmetry arguments, excitation by RCP and LCP light does not lead to any difference ($\widetilde{A} = 0$).

4.3 Atomic multiplet theory for 4f shells

The quasi-atomic character of the lanthanide 4f shell, spatially localized deep within the 'xenon' core, persists even in solids. The 5s and 5d shells provide an efficient screening for the core-like 4f electrons. A well-known consequence is that 4f electrons do not participate in chemical bounding. In addition, the observed 4f multiplet structures in spectroscopic investigations are appropriately described by atomic multiplet theory.

The w electrons of a partially filled shell carry single-particle orbital momenta $\vec{l}_i$, with $i = 1...w$ and spins $\vec{s}_i$. For the lanthanide 4f electrons, coupling of the electron momenta is performed according to the LS (Russel-Saunders) coupling scheme [42], since in the 4f shell of the lanthanides the mutual Coulomb repulsion is dominating over spin-orbit interaction. It is therefore appropriate to first couple the orbital angular momenta, $\vec{l}_i$, to a total orbital angular momentum $\vec{L} = \sum_{i=1}^{w} \vec{l}_i$ as well as all spins, $\vec{s}_i$, to a total spin $\vec{S} = \sum_{i=1}^{w} \vec{s}_i$. The angular momenta $\vec{L}$ and $\vec{S}$ are then coupled by spin-orbit interaction to the total angular momentum, $\vec{J} = \vec{L} + \vec{S}$. The quantum numbers J, L, S, and the magnetic quantum number M describe the corresponding quantum states. Additional quantum numbers, needed for an unambiguous identification of the state, are represented by γ (see below).

Let us consider an electron with orbital angular momentum l that is photoexcited from a (localized) partially filled shell into a continuum state with energy ε and orbital momentum l'. In the photoemission final state $w - 1$ electrons remain in the shell. Due to energy conservation, the PE spectrum gives the replica of the multiplet structure in the PE final state. The electric-dipole transition can be schematically written in the following form:

$$\underbrace{|\, l^w\rangle}_{|J\ M\rangle} \rightarrow \underbrace{\left|l^{w-1}\right\rangle + \left|\varepsilon l'\right\rangle}_{|J'\ M'\rangle} \tag{4.18}$$

In this approach the dipole selection rules $\Delta J = 0, \pm 1$; $\Delta M = 0, \pm 1$ on the total final state govern the transition probabilities. According to Fermi's Golden rule the E1 transition probability from the state $|JM\rangle$ to the total final state $|J'M'\rangle$ can be written as the sum of transition probabilities for different polarizations $q = 0, +1, -1$:

$$\sigma^{JJ'} \propto \sum_q \sigma_q^{JJ'} = \sum_q \left|\left\langle J'M'\right| P_q \left|JM\right\rangle\right|^2, \tag{4.19}$$

where P_q denotes the electric-dipole operator for light polarization q ($P_q = \sqrt{4\pi/3} r Y_1^q(\theta, \varphi)$).

The Wigner-Eckart theorem allows us to separate the partial transition probabilities into radial and angular parts:

$(3j)^2$	$q=0$	$q=\pm1$
$J'=J-1$	$\frac{J^2-M^2}{J(2J-1)(2J+1)}$	$\frac{J(J-1)\pm(2J-1)M+M^2}{2J(2J-1)(2J+1)}$
$J'=J$	$\frac{M^2}{J(J+1)(2J+1)}$	$\frac{J(J+1)\pm M-M^2}{2J(J+1)(2J+1)}$
$J'=J+1$	$\frac{(J+1)^2-M^2}{(2J+3)(J+1)(2J+1)}$	$\frac{(J+1)(J+2)\mp(2J+3)M+M^2}{(2J+3)(J+1)(2J+1)}$

Table 4.2: Expressions for the squared 3j symbols that give the relative weights of E1 transitions from the state $|JM\rangle$.

$$\sigma_q^{JJ'} = \left|\langle J'M'|\, P_q\, |JM\rangle\right|^2 = \underbrace{\left|\langle J'\,\|P\|\,J\rangle\right|^2}_{S_{JJ'}} \begin{pmatrix} J & 1 & J' \\ -M & q & M' \end{pmatrix}^2 . \tag{4.20}$$

The expression in the parentheses denotes a $3j$-symbol, commonly used to describe the coupling of angular momenta. Table 4.2 gives the explicit expressions for the squared $3j$ symbols of all non-vanishing $M \to M'$ transitions. One can see that only transitions with $q = M - M'$ are allowed, because the $3j$ symbol is zero for all other cases ($q \neq M - M'$) . The $3j$ symbols reveal that the light polarization q and the ground-state magnetic quantum number M, and hence the sample magnetization, are directly connected through the dipole selection rules. This is one example showing that experimental determination of line intensities for selected q values gives access to important characteristics of the ground state.

In a simple mean-field picture one can conceive magnetic order to result in a Zeeman splitting of the magnetic sublevels. Below the Curie point, $T \ll T_c$, this splitting is much bigger than the thermal energy $k_B T$. In this limit, only the lowest sublevel $M = -J$ is populated; it is referred to as the ground state. This magnetic splitting of the state $|\gamma LSJM\rangle$ is usually small and can often not be resolved in photoemission; but the unequal population of the M sublevels can become visible in magnetic dichroism experiments.

$(3j)^2$	$q=-1$	$q=0$	$q=+1$
$J'=J-1$	$\frac{1}{2J+1}$	0	0
$J'=J$	$\frac{1}{(J+1)(2J+1)}$	$\frac{1}{(J+1)(2J+1)}$	0
$J'=J+1$	$\frac{1}{(2J+3)(J+1)(2J+1)}$	$\frac{1}{(2J+3)(J+1)}$	$\frac{1}{2J+3}$

Table 4.4: Relative $E1$ transitions probabilities given by the squared $3j$ symbols for excitation from a fully magnetized 4f ground state $|J,-J\rangle$.

The partial transition probabilities from a full-magnetized 4f ground state $|J,-J\rangle$ are given in Table 4.4 for all possible $\Delta M=-1,0,+1$.

Consider for example an experiment in which the sample is in a single domain state $|J,-J'\rangle$, and the incident direction of CP light is chosen collinear with the magnetization. One can see that a reversal of one of them corresponds to a change from, let's say, $\Delta M=+1$ (RCP, $\vec{M}$ parallel to $\vec{q}$) to $\Delta M=-1$ transitions. The light polarization is defined according to the convention used in particle physics, i.e. from the point of view of an observer behind the light. As shown in Table 4.4 only a few total final states can be reached via E1 transitions: there is only one state $|J+1,M-1\rangle$ reached via $\Delta M=-1$, there are two for $\Delta M=0$ and three for $\Delta M=+1$. The statistical weights are very different for different J'. The transitions $\Delta J=-\Delta M$ was found to dominate, e.g. for $\Delta M=+1$ the $|J-1\rangle$ has the highest weight, for $\Delta M=-1$ only the $|J+1\rangle$ is nonzero. Thole [33] has identified this as 'motor' of MD using atomic multiplet theory.

4.4 Specific cases of Gd 4f, Tb 4f

Magnetic dichroism of Gd-4f shell

Seven electrons occupy the Gd-4f shell in the ground state, i.e. the shell is half filled. According to Hund's rules and using the LS coupling scheme (see above),

the orbital angular momenta are coupled to the total angular orbital momentum $L = 0$, and all spins are aligned to give the maximum value of the total spin, $S = 7/2$. The total angular momentum is $J = 7/2$, and the initial state is described by the common designation $^8S_{7/2}$. At low temperatures ($T \to 0$), only the lowest magnetic sublevel $M = -7/2$ is occupied. The matrix-element selection rules allow final-state quantum numbers $J' = 5/2, 7/2, 9/2$, and $M' = -9/2, -7/2, -5/2$. Moreover, the E1 selection rules restrict the allowed final-state orbital quantum number to $L' = 1$, and ignoring the vanishingly small spin-flip probability in non-resonant 4f PE, there is spin conservation, i.e. $S' = S = 7/2$. Also, according to the one-electron selection rule $l' = l \pm 1$ there are only two excitation channels to continuum states. Thus, for an excitation from an f state, only d ($l' = 2$) and g ($l' = 4$) channels are available. After photoionization, the electron configuration of the six electrons left in the 4f shell is denoted by ^7F. In the LS coupling scheme, according to Hund's rule, six electrons are coupled to $L'_{ph} = 3$, $S'_{ph} = 3$, $J'_{ph} = 0, 1, 2, 3, 4, 5, 6$. This means that, in case of Gd, the final-state multiplet consists of the seven multiplet components $^7F_0$ ... $^7F_6$.

It can be shown that the polarization q of the radiation field does not affect the overall transition probability to the dipole-allowed total final state $J' = J - 1,\ J,\ J + 1$ because of $L = 0$ in the Gd 4f ground state [34]. This means that the overall transition probability for excitation from $^8S_{7/2}$ does not depend on the light polarization and, consequently, the total intensity of the ^7F multiplet does not reveal a magnetic dichroism effect. This does not hold for the photoemission intensity distribution inside the multiplet, where particular transition probabilities over the seven final-state components J'_{ph} depend on the total angular momentum J' of the accessible final states (given by the squared $3j$ symbols, see Table 4.2). The J'_{ph} components cannot be fully resolved experimentally (due to their intrinsic widths) so that the redistribution of the total intensity over the seven components – the MD effect – is observed as a change of the multiplet shape. The theoretically expected photoemission intensities over the $^7F_{J'_{ph}}$ multiplet are shown in Fig. 4.4 (T=0 K, full light polarization).

There is a convenient description of experimental data using the concept of the so-called fundamental spectra introduced by Thole and van der Laan [5]. The so-called isotropic spectrum I^0, the magnetic-circular-dichroism spectrum I^1, and the octupole spectrum I^3, are shown in the Fig. 4.5. $I^0$and I^1 are defined in the following way:

$$I^0 = \sum_{J'} \left(\sigma_{-1}^{JJ'} + \sigma_0^{JJ'} + \sigma_{+1}^{JJ'} \right), \tag{4.21}$$

$$I^1 = \sum_{J'} \left(\sigma_{-1}^{JJ'} - \sigma_{+1}^{JJ'} \right). \tag{4.22}$$

It was shown that the magnetic dichroic spectrum I^1 is proportional to the magnetization at any temperature [44]:

$$I^1 \propto \langle M \rangle_{k_B T}. \tag{4.23}$$

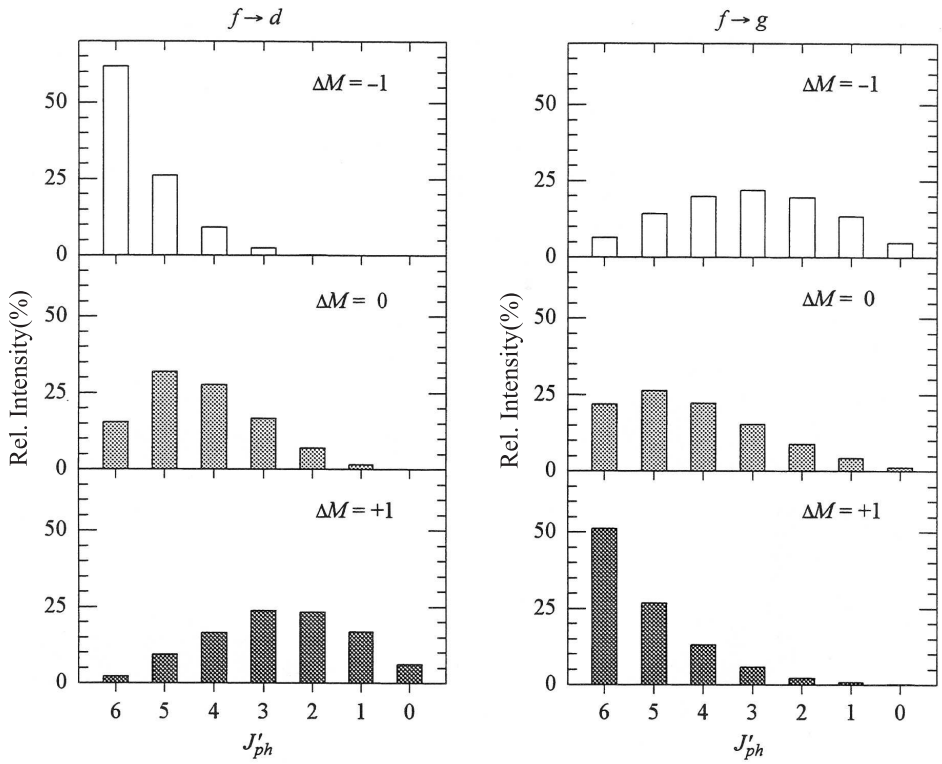

Figure 4.4: Relative intensities of the PE final-state multiplet components for $\triangle M = +1,\ 0,\ -1$; shown transitions are for excitations of d and g waves; from Ref. [43].

We shall utilize this property in the analysis of the magnetic structure in the near-surface region of Gd(0001) and the $p(1 \times 1)O/Gd(0001)$ surface monoxide (see Chapter. 5).

The MD spectra in PE from the Gd-4f shell can be expressed as linear combination of the fundamental spectra. A brief review of atomic multiplet theory describing the PE experiments with circularly and linearly polarized excitation is given in Appendix B. Here, we just reproduce the final expressions for the MD spectrum, derived there for CP and LP polarized excitations.

CP light, for coplanar vectors $\vec{q}, \vec{k}, \vec{M}$:

$$4\pi J^{CP} \approx I^1[(-\frac{3}{7}U^{101} + \frac{30}{49}U^{121}) + I^3(\frac{10}{49}U^{123} - \frac{24}{49}U^{143})], \tag{4.24}$$

with the U^{abx} functions describing the experimental geometry. They can be expressed in terms of trigonometric functions of the angles $\alpha = \angle(\vec{M}, \vec{q})$ and $\beta = \angle(-\vec{M}, \vec{k})$.

LP light, coplanar $\vec{E}$ and $\vec{k}$, and perpendicular $\vec{M}$:

$$4\pi J^{LP} = -(\frac{27}{14}I^1 + \frac{3}{4}I^3 + \frac{15}{112}I^5)R^2R^4 \sin\delta\ \sin 2\alpha, \tag{4.25}$$

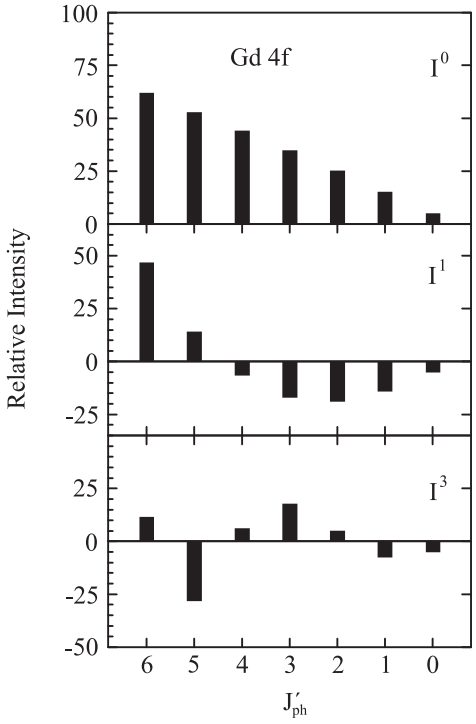

Figure 4.5: Intensity distribution of the fundamental spectra I^x of the Gd $^7F_{J'}$ final-state multiplet: x=0 - isotropic spectrum, x=1 - MCD spectrum, x=3 - octupole spectrum; from Ref. [10].

with $\alpha = \angle(\vec{E}, \vec{k})$. R^c denote radial dipole-matrix elements, the phase shift difference δ between excited photoelectron waves with angular momenta $c = l \pm 1$.

For the ratio of the excitation probabilities for the two possible channels εd and εg, we find (see Ref. [31]):

$$I^0(4f \rightarrow \epsilon g) = I^0(4f \rightarrow \epsilon g) \quad (4.26)$$

$$I^1(4f \rightarrow \epsilon g) = -\frac{4}{3} I^1(4f \rightarrow \epsilon g). \quad (4.27)$$

Magnetic dichroism of Tb 4f shell

In the ground state, the Tb 4f shell is occupied with eight electrons, seven of them have a parallel spin orientation, and one has the opposite spin orientation. Similar to Gd, Hund's rules, in the LS coupling scheme, lead to total angular momenta $L = 3$, $S = 3$, $J = 6$, with the term notation $^7F_6$. In contrast to Gd, photoexcitation from the Tb $^7F_6$ initial state leads to a rich PE final-state multiplet with many components of considerable intensity. Fortunately, the high-spin final-state component $^8S_{7/2}$ is well separated from the rest of the multiplet; it consists of only one line, whose intensity varies strongly for the different light polarizations.

At low temperatures, only the lowest of the (magnetically split) ground-state sublevels $M = -6$ is occupied. The selection rules allow transitions into total final states characterized by $J' = 5, 6, 7$ and $M' = -7, -6, -5$. Similar to the previous case, the selection rule $l' = l \pm 1$ (with initial $l = 3$) allows the two channels $l' = 2, 4$ for the photoelectron. In the final-state, the atom has one electron less and is characterized by $L'_{ph} = 0$, $S'_{ph} = 7/2$, $J'_{ph} = 7/2$. This is equivalent to the Gd configuration in the initial state. The total orbital angular momentum is thus $L' = l'$, resulting from $L'_{ph} = 0$. Moreover, photoexcitation does not affect the total spin $S' = S = 3$ (cf. Gd case, sect.4.4).

J' is restricted (according to the third Hund's rule) by $|L' - S'| \leq J' \leq |L' + S'|$, i.e. $1 \leq J' \leq 5$ in the present case. Taking into account the dipole selection rules, only $J' = 5$ is left for the $f \rightarrow d$ channel; accordingly, the only final state accessible for absorption of circularly polarized light ($q = -1$) is $L' = 2,\ S' = 3,\ J' = 5,\ M' = -5$. For the $f \rightarrow g$ channel, all $J' = 5, 6, 7$ are allowed. Altogether, the relative intensities for different $\triangle M$ transitions are [10]:

$$\left.\begin{array}{c} I(\Delta M = +1) = 1 \\ I(\Delta M = 0) = 0 \\ I(\Delta M = -1) = 0 \end{array}\right\} \; for\ l' = 2 \qquad \left.\begin{array}{c} I(\Delta M = +1) = 1/36 \\ I(\Delta M = 0) = 7/36 \\ I(\Delta M = -1) = 28/36 \end{array}\right\} \; for\ l' = 4.$$